

Electromagnetic absorption of a pinned Wigner crystal at finite temperatures

Hangmo Yi and H.A. Fertig

Department of Physics and Astronomy and Center for Computational Sciences, University of Kentucky, Lexington, Kentucky 40506

(September 8, 2018)

We investigate the microwave absorption of a pinned, two-dimensional Wigner crystal in a strong magnetic field at finite temperatures. Using a model of a uniform commensurate pinning potential, we analyze thermal broadening of the electromagnetic absorption resonance. Surprisingly, we find that the pinning resonance peak should remain sharp *even when the temperature is comparable or greater than the peak frequency*. This result agrees qualitatively with recent experimental observations of the ac conductivity in two-dimensional hole systems in a magnetically induced insulating state. It is shown, in analogy with Kohn's theorem, that the electron-electron interaction does not affect the response of a harmonically pinned Wigner crystal to a spatially uniform external field at any temperature. We thus focus on anharmonicity in the pinning potential as a source of broadening. Using a $1/N$ expansion technique, we show that the broadening is introduced through the self-energy corrections to the magnetophonon Green's functions.

PACS numbers: 73.40.Hm, 73.20.Dx

I. INTRODUCTION

It is now well appreciated that in certain situations, the translational symmetry of an electron gas becomes broken at low temperatures giving rise to an electron solid state called the Wigner crystal (WC).¹ Among other conditions, low density and low disorder are crucial for this novel state to be realized; the inter-electron distance has to be large enough for the Coulomb interaction to dominate the quantum zero-point fluctuations, and the disorder must be weak enough not to destroy the long- (or quasi-long-) range order. One of the systems that satisfy these conditions best is the two-dimensional (2D) electron gas in the GaAs/AlGaAs heterostructure, in which density and disorder can be controlled relatively easily. Furthermore, if a strong magnetic field is applied perpendicular to the 2D plane, the cyclotron motion quenches zero-point fluctuations and the low-density condition is even more easily achieved.²

Although direct observations of the positional order from scattering measurements, for example, have been unattainable, there have been considerable efforts to prove the existence of the WC through more or less indirect methods such as transport measurements³⁻⁹ and photoluminescence.¹⁰⁻¹⁴ One of the most convincing evidences so far is that the 2D systems become insulating when the filling factor $\nu = nhc/eB$ is low: $\lesssim 1/5$ for electron systems³ and $\lesssim 1/3$ for hole systems.⁶ This insulating behavior is generally accepted as a result of pinning of the WC due to impurities. The impurity potential is also supposed to provide a restoring force in the ac electromagnetic response of the WC. If the frequency of the external driving force matches the natural frequency of the pinning mode, a resonance should occur.

Recent experiments on 2D hole systems⁷⁻⁹ have revealed a resonance structure in the ac absorption spectrum in the low filling factor regime. However, some features of the spectrum were qualitatively different from the predictions of the previous calculations based on charge-density-wave (CDW) models;^{15,16} namely, (i) the peak frequency ω_p increased with the magnetic field B , and (ii) the quality factor $Q = \omega_p/\Delta\omega$ was found to be as large as 30 in some data.⁹ The CDW calculations had predicted that ω_p would decrease with B and the peak would be much broader ($Q \sim 1$).

These puzzling experimental findings were later examined by the authors of Refs. 17 and 18. Based on weak disorder models at $T = 0$, they found that (i) was explained if the disorder potential was allowed to vary within a magnetic length $l_0 = \sqrt{\hbar c/eB}$. This short-length-scale physics is missing in the previous CDW calculations since they assume that the disorder potential can vary only in a length scale longer than the lattice periodicity a . (In the experiments in Refs. 7, 8, and 9, $a > l_0$.) More specifically, in Ref. 18, it was suggested that the roughness of the GaAs/AlGaAs interface could serve as a source of such a short-length-scale disorder potential. A "pit" on the interface, which is typically several atoms wide, can trap an electron by allowing it to stay closer to the positively charged donor plane and gain electrostatic energy. In a strong magnetic field, one can project the many-body wave function onto the lowest Landau level (LLL). Assuming $a \gg l_0$, one may ignore exchange energy and describe the many-body ground state as a Hartree-type product of single electron wave packets of size $\sim l_0$, which are, in the absence of disorder, located at crystal lattice sites.¹⁹ Suppose an electron wave packet is situated right on a pit. Since its size decreases with increasing B , the probability for the electron to stay inside the pit subsequently increases, provided *the pit size*

is smaller than l_0 . Since ω_p is essentially given by the expectation value of the pinning potential strength, the above cartoon picture explains how ω_p grows with B . In addition, as described below, the long-range Coulomb interaction suppresses low-energy collective excitations and leads to a sharp resonance.

At finite temperatures, however, thermal fluctuations should broaden the resonance peak. One important observation is that the peaks measured in experiments keep getting narrower down to the lowest T measured. This suggests that the main source of broadening is thermal fluctuations. Interestingly, the experiments also find that $\Delta\omega \ll T$ even though $T \gtrsim \omega_p$. Thus, how the thermal broadening comes about is a highly non-trivial question. We address the question in this paper. As the thermal broadening is the main issue, we will simplify the disorder model and assume that the pinning centers themselves form exactly the same lattice as the WC. We also assume that the impurity potential has the same strength at all sites.²⁰ Several different disorder potentials — including the uniform commensurate model we will use in this work — have been studied at $T = 0$ in a previous study,¹⁸ but it was found that the details of disorder do not alter the resonance structure qualitatively. We believe the thermal behavior is not sensitive to details of disorder, either.

Our result can be summarized as follows. In order to understand low, but finite temperature behavior, one needs to investigate the low-energy excitations and their interactions. The longitudinal and the transverse phonon modes of the WC mix together in a strong magnetic field and two new normal modes, magnetophonons and magnetoplasmons, emerge.^{21–23} We focus on the magnetophonons because the energy of the other mode, magnetoplasmons, is essentially given by the cyclotron energy $\hbar\omega_c = \hbar eB/mc$, which is a few orders of magnitude greater than T and ω_p . In a theory that treats displacement of electrons from lattice sites harmonically, magnetophonons are independent and produces only a delta-function peak in the ac absorption spectrum. The interaction between magnetophonons comes about from anharmonicity of the Hamiltonian. There are two sources of anharmonicity in our model: Coulomb interaction and pinning potential. Since the external ac field has a much larger wave length ($\gtrsim 1$ m) than the size of the system (typically $\sim 10^{-5}$ m),⁷ it is safe to treat it as a uniform field that couples only to the center-of-mass degree of freedom. If the pinning potential is completely harmonic, we find that the anharmonicity in the Coulomb interaction does not contribute to the absorption spectrum, because the interaction depends only on the relative position of electrons. This is analogous to the Kohn's theorem,²⁴ which states that the electron-electron interaction does not affect the cyclotron frequency in a disorder-free system. The theorem remains true even in a harmonically pinned WC. Therefore, anharmonicity of the pinning potential is crucial for understanding thermal broadening.

As will be shown below, magnetophonon modes are very closely related to angular momentum excitations. It is therefore natural to exploit analogies to 2D spin lattice systems. In fact, written in magnetophonon creation and annihilation operators, our model Hamiltonian resembles that of an $SU(N)$ Schwinger boson formulation of a 2D quantum (anti-)ferromagnet.^{25–27} Further utilizing this analogy, we use a $1/N$ expansion technique that has proved useful in spin systems. Not only does it provide a systematic way of collecting important processes in Feynman diagrams, but also its lowest-order mean-field (MF) solution already contains terms that are higher order in coupling constant in a standard diagrammatic many-body calculation. Importantly, the position of absorption resonance peak is mostly determined at the MF level.

The Coulomb interaction and the pinning potential affect the spectrum of the magnetophonons significantly. Without pinning, the dispersion relation is well known to take the form $\varepsilon_{\mathbf{q}} \propto |\mathbf{q}|^{3/2}$ in the long wave length limit, calculated both classically²¹ and quantum mechanically^{28,19}. In the uniform commensurate pinning model, it is modified to $\varepsilon_{\mathbf{q}} \approx V + v_s|\mathbf{q}|$, where V represents the strength of the pinning potential and v_s is the sound velocity of the magnetophonon mode. The new spectrum is not only gapped, but also makes the density of states (DOS) vanish linearly in the low-energy limit. It turns out that the slope of the low energy DOS is so small that there are extremely few low-energy excitation modes about ω_p . As a consequence, we find that the thermal fluctuations are substantially suppressed and the peak remains sharp.

This paper is organized as follows. The magnetophonon creation and annihilation operators are constructed out of displacement operators in the LLL in Sec. II. We derive the ac conductivity in terms of magnetophonon Green's functions in Sec. III. We then introduce in Sec. IV, the Hamiltonian of the WC, and derive in Sec. V, a generalized Kohn's theorem that explains why the anharmonicity in the Coulomb interaction does not contribute to thermal shift or broadening of the absorption spectrum in a harmonic pinning model. Sec. VI is devoted to $1/N$ expansion calculations of the Green's functions. We present the results in Sec. VII, and finally conclude with a discussion in Sec. VIII. Details of some calculations are given in Appendices.

II. MAGNETOPHONONS

Before we write down the Hamiltonian in a second-quantized form, it is helpful to see how the Hilbert space is spanned by the eigenfunctions of magnetoplasmon and magnetophonon number operators. In the circular gauge,

$\mathbf{A} = (1/2)\mathbf{B} \times \mathbf{r}$, a 2D single electron wavefunction in the n -th Landau level with angular momentum quantum number m takes the form

$$\psi_{nm}(\mathbf{r}) = \frac{(-\sqrt{2}l_0)^{2n+m}}{\sqrt{2\pi l_0^2 n!(n+m)!}} e^{\frac{|z|^2}{4l_0^2}} \partial_z^n \partial_{z^*}^{n+m} e^{-\frac{|z|^2}{2l_0^2}}, \quad (2.1)$$

where $z = x + iy$, $\partial_z = (\partial/\partial x - i\partial/\partial y)/2$, $\partial_{z^*} = (\partial/\partial x + i\partial/\partial y)/2$, and $l_0 = \sqrt{\hbar c/eB}$ is the magnetic length. This wavefunction spans the entire single particle Hilbert space. It is now useful to define ladder operators that raise or lower n and m . We define the Landau level raising operator

$$a^\dagger = \frac{1}{\sqrt{2}} \left(\frac{z^*}{2l_0} - 2l_0 \partial_z \right), \quad (2.2)$$

and the angular momentum raising operator

$$b^\dagger = \frac{1}{\sqrt{2}} \left(\frac{z}{2l_0} - 2l_0 \partial_{z^*} \right). \quad (2.3)$$

It is straightforward to show that

$$\begin{aligned} a^\dagger \psi_{nm} &\propto \psi_{n+1, m-1}, & a \psi_{0m} &= 0, \\ b^\dagger \psi_{nm} &\propto \psi_{n, m+1}, & b \psi_{n, -n} &= 0, \\ [a, a^\dagger] &= [b, b^\dagger] = 1, \\ [a, b] &= [a^\dagger, b^\dagger] = [a, b^\dagger] = [a^\dagger, b] = 0. \end{aligned} \quad (2.4)$$

In what follows, the above ladder operators will be defined at each WC lattice site. Then, a Fourier transformed operator $a_{\mathbf{q}}^\dagger$ will serve as a magnetoplasmon creation operator, and $b_{\mathbf{q}}^\dagger$ as a magnetophonon creation operator. We will use the latter terms to refer to the a^\dagger and b^\dagger operators from this point on.

In the low filling factor limit, the Landau gap $\hbar\omega_c$ is large, so one can safely truncate the Hilbert space and work in the LLL only. Furthermore, the ground state of the WC in this limit is believed to be well represented by a product of a collection of zero angular momentum single particle wave functions, each of which is centered at a lattice site.¹⁹ This is analogous to a Hartree wave function. Although the single particle wave functions are not orthogonal, their overlap is exponentially small if $l_0 \ll a$. Thus, one may ignore exchange energy correction and the wave functions do not have to be antisymmetrized. In other words, electrons are distinguishable because each one of them is strongly localized at a lattice site far from the others. For higher angular momentum states, the size of wave packets grow with m . However, the above argument should be still valid for the first few higher angular momentum states. Therefore, we assume that the Hilbert space is given by a direct product of single particle Hilbert spaces spanned by angular momentum states in the LLL.

Due to the strong Coulomb repulsion, we assume that there is only one electron per site. This allows us to label each many-body energy eigenstate by a collection of N_s angular momentum quantum numbers or magnetophonon occupation numbers, where N_s is the total number of sites. As will be shown below, the above statement is not exactly true, because in reality, different angular momentum states mix together due to quantum fluctuations. This is demonstrated in our Hamiltonian as terms that do not conserve the magnetophonon number. Nonetheless, higher angular momentum mixing is small at low temperatures and the above argument should be a good qualitative description of the system.

The many-body wavefunction is written as¹⁹

$$\Psi(\{\mathbf{r}_i\}) = \prod_i \psi_{m_i}(\mathbf{r}_i; \mathbf{R}_i), \quad (2.5)$$

where the single particle wavefunction $\psi_{m_i}(\mathbf{r}_i; \mathbf{R}_i)$ is localized at a lattice site \mathbf{R}_i and has an angular momentum quantum number m_i . More specifically, it may be written as

$$\psi_m(\mathbf{r}_i; \mathbf{R}_i) = \frac{1}{\sqrt{2\pi l_0^2 m!}} \left(\frac{z_i - Z_i}{\sqrt{2}l_0} \right)^m e^{-\frac{|z_i - Z_i|^2}{4l_0^2}} e^{\frac{z_i Z_i^* - z_i^* Z_i}{2l_0^2}}, \quad (2.6)$$

where $Z_i = R_i^x + iR_i^y$. Note that the last exponential is a pure phase and is needed to keep the wavefunction in the LLL. We will assume that $\{\mathbf{R}_i\}$ forms a triangular lattice in the ground state. The ladder operators in Eqs. (2.2) and (2.3) are modified at each lattice site and may be written as

$$a_i^\dagger = \frac{1}{\sqrt{2}} \left(\frac{\zeta_i^* + Z_i^*}{2l_0} - 2l_0 \partial_{\zeta_i} \right), \quad (2.7)$$

$$b_i^\dagger = \frac{1}{\sqrt{2}} \left(\frac{\zeta_i - Z_i}{2l_0} - 2l_0 \partial_{\zeta_i^*} \right), \quad (2.8)$$

where $\zeta_i = z_i - Z_i$ is the complex notation of the displacement of the i th electron from its site.

In terms of the above ladder operators, the original electron position is written as

$$x_i = R_i^x + \frac{l_0}{\sqrt{2}}(b_i + b_i^\dagger + a_i + a_i^\dagger), \quad (2.9)$$

$$y_i = R_i^y + \frac{l_0}{\sqrt{2}}(-b_i + b_i^\dagger + a_i - a_i^\dagger). \quad (2.10)$$

When an operator is applied only to states that are completely in the LLL, it may be represented by a “LLL-projected” operator. In the above expression, this means simply dropping the magnetoplasmon operators a_i and a_i^\dagger that couples the LLL states to higher Landau levels. The projected operators then take the form

$$x_i = R_i^x + \frac{l_0}{\sqrt{2}}(b_i + b_i^\dagger), \quad (2.11)$$

$$y_i = R_i^y + \frac{l_0}{\sqrt{2}}(-b_i + b_i^\dagger). \quad (2.12)$$

The above operators satisfy the usual LLL commutation relation²⁹

$$[x_i, y_j] = l_0^2 \delta_{ij}. \quad (2.13)$$

III. CONDUCTIVITY

The quantity we will eventually compute is the ac conductivity tensor $\sigma^{\mu\nu}(\omega)$, where $\mu, \nu = x, y$. In this section, we will show how $\sigma^{\mu\nu}(\omega)$ is derived in terms of the magnetophonon Green’s functions.

The external perturbation due to a spatially uniform electric field with frequency ω is $H'(t) = e \text{Re} e^{-i\omega t} \mathbf{E}_0 \cdot \sum_i \mathbf{u}_i$, where $\mathbf{u}_i = \mathbf{r}_i - \mathbf{R}_i$. In the linear response theory, the electric current is given by

$$j^\mu(t) = \text{Re} \frac{i\omega e \rho_0}{N_s} \sum_i \langle u_i^\mu(t) \rangle \quad (3.1)$$

$$= \text{Re} \frac{i\omega e \rho_0}{N_s} \sum_i \left(-\frac{i}{\hbar} \right) \int dt' \theta(t-t') \langle [u_i^\mu(t), H'(t')] \rangle \quad (3.2)$$

$$= \text{Re} \frac{i\omega e^2 \rho_0}{\hbar} e^{-i\omega t} \chi_R^{\mu\nu}(\omega) E_0^\nu, \quad (3.3)$$

where ρ_0 is the 2D number density of electrons. The brackets $\langle \dots \rangle$ denote a thermal average for the unperturbed Hamiltonian and the zero wave vector response function is defined as

$$\chi_R^{\mu\nu}(\omega) = \int dt' e^{i\omega(t-t')} \theta(t-t') \langle [u_{\mathbf{q}=\mathbf{0}}^\mu(t), u_{\mathbf{q}=\mathbf{0}}^\nu(t')] \rangle. \quad (3.4)$$

The linear ac conductivity can be read off from Eq. (3.3) as

$$\sigma^{\mu\nu}(\omega) = -\text{Im} \frac{\omega e^2 \rho_0}{\hbar} \chi_R^{\mu\nu}(\omega). \quad (3.5)$$

In general, one has to include the polarization field in the calculation and solve for the conductivity self-consistently. In a system with uniform background charge, however, the $\mathbf{q} = \mathbf{0}$ component of the polarization is meaningful only on the boundaries. In 2D, the boundary effect dies off inversely with the size of the system, and may be ignored in the thermodynamic limit.

The response function $\chi_R^{\mu\nu}$ may be most easily obtained by computing the Matsubara frequency response function

$$\chi^{\mu\nu}(i\omega_n) = -i \int dt' e^{i\omega_n \tau} \langle T_\tau u_{\mathbf{q}=0}^\mu(\tau) u_{\mathbf{q}=0}^\nu(0) \rangle \quad (3.6)$$

and then analytically continuing

$$\chi_R^{\mu\nu}(\omega) = \chi^{\mu\nu}(i\omega_n \rightarrow \omega + i0^+), \quad (3.7)$$

where T_τ denotes time-ordering in the imaginary time τ . Since $u_i^\mu = r_i^\mu - R_i^\mu$ is a linear combination of b_i and b_i^\dagger as in Eqs. (2.11) and (2.12), $\chi^{\mu\nu}(i\omega_n)$ can be written in terms of magnetophonon Green's functions as

$$\begin{aligned} \chi^{\mu\nu} &= \begin{bmatrix} \chi^{xx} & \chi^{xy} \\ \chi^{yx} & \chi^{yy} \end{bmatrix} \\ &= \frac{l_0^2}{2} \begin{bmatrix} 1 & 1 \\ i & -i \end{bmatrix} \begin{bmatrix} G^{--} & G^{+-} \\ G^{++} & G^{+-} \end{bmatrix} \begin{bmatrix} 1 & -i \\ 1 & i \end{bmatrix}. \end{aligned} \quad (3.8)$$

The Green's functions are defined as

$$\begin{bmatrix} G^{--} & G^{+-} \\ G^{++} & G^{+-} \end{bmatrix} = - \int d\tau e^{i\omega_n \tau} \left\langle T_\tau \begin{bmatrix} bb^\dagger & bb \\ b^\dagger b^\dagger & b^\dagger b \end{bmatrix} \right\rangle, \quad (3.9)$$

where bb^\dagger should be interpreted as $b(\tau)b^\dagger(0)$, etc.

IV. HAMILTONIAN

The discussions so far have been quite general and independent of the actual Hamiltonian of the system. In this section, we will construct the Hamiltonian in terms of magnetophonon operators. Let us first consider a WC without disorder. The kinetic part of the Hamiltonian is given by

$$H_k = \frac{\hbar^2}{2m} \left(\nabla + \frac{e}{c} \mathbf{A} \right)^2 \quad (4.1)$$

$$= \hbar\omega_c \left(a_i^\dagger a_i + \frac{1}{2} \right), \quad (4.2)$$

where a_i^\dagger is the magnetoplasmon creation operator in Eq. (2.7). The Coulomb interaction takes the form

$$H_C = \frac{1}{2} \sum_{i \neq j} \frac{e^2}{\kappa |\mathbf{r}_i - \mathbf{r}_j|}, \quad (4.3)$$

where κ is the dielectric constant. Expanded in terms of the displacement \mathbf{u}_i , the above equation may be written as

$$H_C = \frac{1}{2} \sum_{i \neq j} \sum_{\mu\nu} u_i^\mu P_{ij}^{\mu\nu} u_j^\nu + \text{const.} + \mathcal{O} \left[\left(\frac{u}{a} \right)^3 \right], \quad (4.4)$$

where $\mu, \nu = x, y$, and a is the lattice constant. The dynamic matrix is given by

$$P_{ij}^{\mu\nu} = \frac{e^2}{\kappa |\mathbf{R}_{ij}|^3} \left(\delta_{\mu\nu} - 3 \frac{R_{ij}^\mu R_{ij}^\nu}{|\mathbf{R}_{ij}|^2} \right), \quad (4.5)$$

where $\mathbf{R}_{ij} \equiv \mathbf{R}_i - \mathbf{R}_j$.

Now we take the strong-magnetic-field limit and project the above Hamiltonian to the LLL. Technically, this means rewriting it in terms of ladder operators in Eqs. (2.7) and (2.8), and abandoning any term that is normal-ordered in a^\dagger and a , i.e., any term in which all a 's are placed to the right of all a^\dagger 's. Obviously, the kinetic term is constant after the projection, and may be ignored. The Coulomb interaction may be rewritten as

$$\begin{aligned} H_{C2} &= - \sum_{i \neq j} \frac{e^2 l_0^2}{4 |\mathbf{R}_{ij}|^3} \left[b_i^\dagger b_j + b_i b_j^\dagger + 3 \left(n_{ij}^2 b_i b_j + n_{ij}^{*2} b_i^\dagger b_j^\dagger \right) \right] \\ &\quad + \sum_i \left(\sum_{j(\neq i)} \frac{e^2 l_0^2}{2 |\mathbf{R}_{ij}|^3} \right) b_i^\dagger b_i, \end{aligned} \quad (4.6)$$

where $n_{ij} \equiv (R_{ij}^x + iR_{ij}^y)/|\mathbf{R}_{ij}|$. The above expression may also be derived by making use of the analogy between the electron system and a spin-lattice system (see Ref. 18). Note that rewriting Eq. (4.4) into Eq. (4.6), we have dropped not only a constant term, but also the last term that is anharmonic. In fact, in order to investigate thermal broadening, it is necessary to keep at least one anharmonic term in the Hamiltonian, because a completely harmonic Hamiltonian would lead to a theory of free independent eigenmodes and all correlation functions would be temperature independent. However, the anharmonic terms in the Coulomb interaction do *not* contribute to thermal shift or broadening of the response function to a spatially uniform external perturbation in a harmonic pinning model. This is a highly non-trivial statement, which we discuss in the next section. As a consequence of this, we are led to investigate anharmonicity in the other term in the Hamiltonian: the pinning potential.

For simplicity, we consider only the uniform commensurate pinning model in this work. In reality, of course, disorder is more complicated in several ways. First, non-commensurate or non-uniform disorder will break the discrete translational symmetry and deform the lattice. Unless the impurity potential is exactly circular at each site, it will also mix different angular momentum states.

However, it was shown in Ref. 18 that at $T = 0$, the uniform commensurate pinning model yields qualitatively the same result as more complicated disorder models. Furthermore, experimental data show that the resonance peaks keep getting narrower down to $T \lesssim \hbar\omega_p$, suggesting that thermal fluctuation affects broadening more than disorder does, at least at the observed temperatures. Therefore, we believe this simple disorder model is sufficient for our purpose.

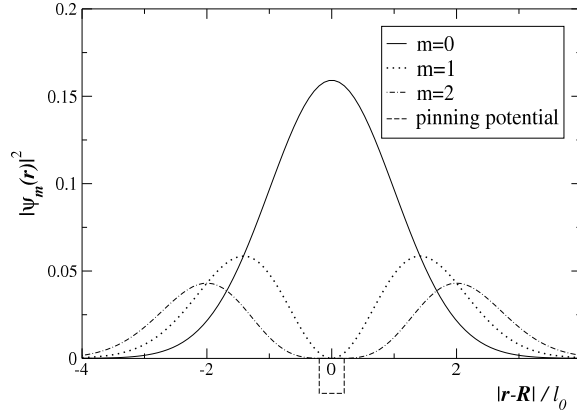


FIG. 1. Probability $|\psi_m(\mathbf{r})|^2$ of single particle wave functions in the lowest Landau level. A pit is also schematically drawn (a square well at the origin) in order to emphasize that we are considering the case in which the pit size $< l_0$. States with $m > 0$ have little overlap with the pit.

Fig. 1 shows a schematic picture of the probability function for the three lowest angular momentum states centered at an interface pit. Since states with $m > 0$ have little probability to reside in the pit, they are not affected by it. The pinning Hamiltonian is thus appropriately described in terms of magnetophonon operators by

$$H_p = -V \sum_i \delta_{b_i^\dagger b_i, 0}, \quad (4.7)$$

where V is the amount of energy an electron pays to move from $m = 0$ state to a higher angular momentum state *in the absence of Coulomb interaction*. This potential is highly anharmonic, and the resulting phonon problem is exceedingly difficult to analyze. To overcome this, we adopt an approximate form of the pinning potential.

The simplest choice that includes anharmonicity is

$$H_{p4} = -\frac{V}{2} \sum_i (1 - b_i^\dagger b_i)(2 - b_i^\dagger b_i), \quad (4.8)$$

which takes the same value as H_p at $b_i^\dagger b_i = 0, 1$, and 2 . At first, the above Hamiltonian looks problematic because it has no lower bound. As will be shown below, however, the $1/N$ expansion is well defined provided the thermal average $\langle b_i^\dagger b_i \rangle < 1$. It turns out that $\langle b_i^\dagger b_i \rangle$ is indeed small and this approximation gives sensible results in the observed temperature range $T \lesssim 10\hbar\omega_p$.

Finally, the total Hamiltonian of our model is given by

$$H = H_{C2} + H_{p4}. \quad (4.9)$$

A similar Hamiltonian was derived in Ref. 18 by limiting the Hilbert space to two angular momentum states per site and writing the Hamiltonian in a pseudospin representation. Although the higher-angular-momentum states should not affect low temperature behavior qualitatively, and the assumption that the many-body wave function takes a simple product form breaks down for large m_i , the above Hamiltonian has been derived without restricting the Hilbert space to a fixed number of states per site.

V. GENERALIZED KOHN'S THEOREM

In this section, we will derive a generalized Kohn's theorem, which guarantees that the anharmonicity in the Coulomb interaction does not alter the absorption spectrum of a uniform electromagnetic field for a harmonically and uniformly pinned model. Similar generalizations have been made in the context of an electron gas in a parabolic potential in Refs. 30 and 31.

Before we present the proof, let us take a brief look at the original Kohn's theorem. In a magnetic field, the energy spectrum of a single free electron is simply given by Landau levels. Now, suppose that there are many electrons interacting with one another via Coulomb or any other interaction. Kohn's theorem tells us that the electromagnetic absorption spectrum of such a system, as measured through a response to a spatially uniform external field, will be exactly the same as that of a single electron. The proof of this theorem is disarmingly simple. Since the electron-electron interaction depends only on the relative degrees of freedom, it commutes with the center-of-mass motion. Therefore, the observed center-of-mass spectrum is not affected by the interaction at all.

The big difference in the problem considered in this paper is that there is pinning. However, a similar argument can be established in a special case of harmonic uniform pinning model. Suppose that the pinning Hamiltonian takes the form

$$H_{\text{har}} = V \sum_i b_i^\dagger b_i \quad (5.1)$$

$$= V \sum_{\mathbf{q}} b_{\mathbf{q}}^\dagger b_{\mathbf{q}}. \quad (5.2)$$

Since this Hamiltonian is separable in different momenta \mathbf{q} , its eigenstates may be written as a product of the form

$$|\Psi\rangle = |\Psi_{\text{CM}}\rangle |\Psi_{\text{rel}}\rangle, \quad (5.3)$$

where $|\Psi_{\text{CM}}\rangle$ is an eigenstate of the center-of-mass operator $b_{\mathbf{q}=\mathbf{0}}^\dagger b_{\mathbf{q}=\mathbf{0}}$ and $|\Psi_{\text{rel}}\rangle$ of all the other relative degrees of freedom.

Suppose that we calculate the ac conductivity of a *non-interacting* electron system using the expressions in Sec. III. In order to compute the thermal average, one needs to compute the expectation values over the above eigenstates. We make an important observation here that the conductivity depends only on $|\Psi_{\text{CM}}\rangle$, because the operators in Eq. (3.4) are functions only of $b_{\mathbf{q}=\mathbf{0}}^\dagger$ and $b_{\mathbf{q}=\mathbf{0}}$.

Now let us add the Coulomb interaction as in Eq. (4.3) to the Hamiltonian. As H_C depends only on relative degrees of freedom, it obviously commutes with the center-of-mass displacement

$$\mathbf{u}_{\text{CM}} = \frac{1}{N_s} \sum_i \mathbf{u}_i. \quad (5.4)$$

In terms of magnetophonon operators, it implies

$$[H_C, b_{\mathbf{q}=\mathbf{0}}^\dagger b_{\mathbf{q}=\mathbf{0}}] = 0. \quad (5.5)$$

Therefore, the Coulomb interaction does not alter the spectrum of $|\Psi_{\text{CM}}\rangle$, although it may (and in general, it does) alter that of $|\Psi_{\text{rel}}\rangle$. Since the ac conductivity is determined by the spectrum of $|\Psi_{\text{CM}}\rangle$ alone, it is unaltered by the presence of the Coulomb interaction. This completes the proof of the generalized Kohn's theorem.

This theorem implies that if we use a harmonic pinning potential, the contribution from the anharmonic Coulomb interaction terms in Eq. (4.4) to the uniform response function will *vanish in all orders* of u/a . Therefore, we will use a harmonic Hamiltonian for Coulomb interaction, but an anharmonic one for pinning potential, hence the total Hamiltonian is given as in Eq. (4.9). The detailed analysis of the anharmonic pinning potential will be given below, using a $1/N$ expansion technique.

VI. $1/N$ EXPANSION

A $1/N$ expansion technique consists of three steps. First, we make N copies of the magnetophonon operators. Second, using a Hubbard-Stratonovich (HS) decoupling technique, the anharmonic terms are replaced by products of a harmonic term and an auxiliary HS field. Finally, we expand the magnetophonon Green's function in powers of $1/N$. In principle, the expansion is exact if all orders of $1/N$ are kept. Instead, as is conventionally done, we will stop at the first order to get an approximation. Before going into details, it should be noted that N will be set equal to 1 at the end of the approximation, therefore it is not a perturbative expansion in any sense. However, this technique usually does a better job in systematically picking out important processes than many other many-body techniques. In fact, the zeroth order approximation, which is a harmonic theory with magnetophonons coupled to the MF value of the HS field, already contains the RPA contribution. The first order approximation adds self-energy corrections to the Green's functions and gives us a thermal broadening.

After replication, Eq. (4.9) becomes

$$H = \sum_{l=1}^N H_{C2}(\{b_{li}, b_{li}^\dagger\}) + V \sum_{li} b_{li}^\dagger b_{li} - \frac{V}{2N} \sum_{l_1 l_2 i} b_{l_1 i}^\dagger b_{l_2 i}^\dagger b_{l_2 i} b_{l_1 i}, \quad (6.1)$$

where l , l_1 , and l_2 are species indices. H_{C2} is the same as in Eq. (4.6) with different magnetophonon operators substituted for each species. There is an extra factor of $1/N$ in the last term because it involves two species summations. Note that the above equation has been normal-ordered. In this form, we may recast the problem in a path-integral form simply by replacing b (b^\dagger) by a classical field $z(\tau)$ ($z^*(\tau)$) in the imaginary time $\tau = it$. The Euclidean action is given by

$$S = \int d\tau \left\{ \sum_{li} z_{li}^*(\tau) \partial_\tau z_{li}(\tau) + \sum_l H_{C2}(\{z_{li}(\tau), z_{li}^*(\tau)\}) + V \sum_{li} |z_{li}(\tau)|^2 - \frac{V}{2N} \sum_i \left[\sum_l |z_{li}(\tau)|^2 \right]^2 \right\}. \quad (6.2)$$

The first term is the usual Berry phase in the imaginary time.

In the second step, we introduce a real HS field $Q_i(\tau)$ to decouple the quartic term. The procedure is formally expressed in a functional integral form as

$$\begin{aligned} & \exp \left[\int d\tau \frac{V}{2N} \left(\sum_l |z_{li}|^2 \right)^2 \right] \\ &= c \int \mathcal{D}Q_i \exp \left[- \int d\tau \frac{V}{2} \left(-2Q_i \sum_l |z_{li}|^2 + NQ_i^2 \right) \right], \end{aligned}$$

where c is a constant. Then the generating functional written in terms of both z and Q takes the form

$$Z \equiv \int \mathcal{D}^2 z \mathcal{D}Q e^{-S_{\text{HS}}}, \quad (6.3)$$

where

$$\begin{aligned} S_{\text{HS}} = \int d\tau & \left[\sum_{li} z_{li}^* \partial_\tau z_{li} + \sum_l H_{C2}(\{z_{li}, z_{li}^*\}) \right. \\ & \left. + V \sum_{li} (1 - Q_i) |z_{li}|^2 + \sum_i \frac{NV}{2} Q_i^2 \right]. \end{aligned} \quad (6.4)$$

$\mathcal{D}^2 z$ denotes functional integral over real and imaginary parts of z field. So far the action contains all orders of $1/N$ and is therefore exact. In the following subsections, we will Taylor-series expand it in powers of $1/N$.

A. Mean field theory

As is the usual practice,²⁶ we assume that the MF solution of $Q_i(\tau)$ is independent of i and τ (Ref. 32). Since the crystal momentum \mathbf{q} is still a good quantum number, it is useful to Fourier-transform the action. We define

$$z_{lq} = \frac{1}{\beta\sqrt{N_s}} \int d\tau \sum_i e^{i\omega_n\tau - i\mathbf{q}\cdot\mathbf{R}_i} z_{li}, \quad (6.5)$$

where q is a shorthand notation for $(i\omega_n, \mathbf{q})$ and β is the inverse temperature. In terms of the above Fourier components, the MF action is given by

$$S_{\text{MF}}(\bar{Q}) = \beta \sum_l \sum_q \left[(-i\omega_n + f_{\mathbf{q}}) z_{lq}^* z_{lq} - \frac{1}{2} (g_{\mathbf{q}} z_{l, -q} z_{lq} + g_{\mathbf{q}}^* z_{lq}^* z_{l, -q}^*) \right], \quad (6.6)$$

where

$$f_{\mathbf{q}} = (1 - \bar{Q})V + \frac{1}{2} \sum_{\mathbf{R}_j \neq 0} (1 - e^{-i\mathbf{q}\cdot\mathbf{R}_j}) \frac{e^2 l_0^2}{|\mathbf{R}_{ij}|^3}, \quad (6.7)$$

$$g_{\mathbf{q}} = \frac{3}{2} \sum_{\mathbf{R}_j \neq 0} e^{-i\mathbf{q}\cdot\mathbf{R}_j} \frac{e^2 l_0^2}{|\mathbf{R}_{ij}|^3} n_i^2. \quad (6.8)$$

The MF Green's functions take the form

$$\begin{bmatrix} G^{+-} & G^{--} \\ G^{++} & G^{+-} \end{bmatrix} = \frac{1}{\omega_n^2 + f_{\mathbf{q}}^2 - |g_{\mathbf{q}}|^2} \begin{bmatrix} -i\omega_n - f_{\mathbf{q}} & g_{\mathbf{q}}^* \\ g_{\mathbf{q}} & i\omega_n - f_{\mathbf{q}} \end{bmatrix}. \quad (6.9)$$

We choose the MF value \bar{Q} in such a way that the MF free energy

$$F_{\text{MF}}(\bar{Q}) = -\ln \int \mathcal{D}^2 z e^{-S_{\text{MF}}(\bar{Q})} \quad (6.10)$$

has a saddle point. Solving $\partial F_{\text{MF}}/\partial \bar{Q} = 0$, we get

$$\bar{Q} = \frac{1}{N_s} \sum_{\mathbf{q}} \frac{\int \mathcal{D}^2 z e^{-S_{\text{MF}}(\bar{Q})} z_{\mathbf{q}}^* z_{\mathbf{q}}}{\int \mathcal{D}^2 z e^{-S_{\text{MF}}(\bar{Q})}}. \quad (6.11)$$

Note that \bar{Q} above is equal to the thermally averaged value of the number of magnetophonons per site, $n_{\text{ph}} \equiv \sum_{\mathbf{q}} \langle b_{\mathbf{q}}^\dagger b_{\mathbf{q}} \rangle / N_s$. \bar{Q} has to be determined self-consistently and is a function of temperature. Note that $f_{\mathbf{q}} > 0$ for all \mathbf{q} if $n_{\text{ph}} < 1$. This implies that the MF theory is stable when there are not too many magnetophonons. The instability in the many-magnetophonon regime signals the onset of a “depinning transition.” In fact, this instability is an artifact caused by the fact that our choice of the pinning potential H_{p4} in Eq. (4.8) has no lower bound. However, we believe there is indeed a depinning transition in real situations, and it is appropriate to regard $n_{\text{ph}}^c = 1$ as the critical number of magnetophonons at the transition in this model. As we go beyond the MF theory and include higher orders in $1/N$, n_{ph} decreases due to fluctuations in Q_i .

Since the MF action S_{MF} is quadratic, it may be diagonalized using a Bogoliubov transformation. It is more convenient to work in the Hamiltonian representation. The Hamiltonian that reproduces S_{MF} is

$$H_{\text{MF}} = \sum_{\mathbf{q}} \left[f_{\mathbf{q}} b_{\mathbf{q}}^\dagger b_{\mathbf{q}} - \frac{1}{2} \left(g_{\mathbf{q}} b_{-\mathbf{q}} b_{\mathbf{q}} + g_{\mathbf{q}}^* b_{\mathbf{q}}^\dagger b_{-\mathbf{q}}^\dagger \right) \right]. \quad (6.12)$$

We define a new boson annihilation operator

$$\gamma_{\mathbf{q}} = u_{\mathbf{q}} b_{\mathbf{q}} + v_{\mathbf{q}} b_{-\mathbf{q}}^\dagger. \quad (6.13)$$

In order to ensure the boson statistics, it has to satisfy

$$[\gamma_{\mathbf{q}}, \gamma_{\mathbf{q}}^\dagger] = |u_{\mathbf{q}}|^2 - |v_{\mathbf{q}}|^2 = 1. \quad (6.14)$$

By setting

$$u_{\mathbf{q}} = e^{i\phi_{\mathbf{q}}} \sqrt{\frac{1}{2} \left(\frac{f_{\mathbf{q}}}{\varepsilon_{\mathbf{q}}} + 1 \right)}, \quad (6.15)$$

$$v_{\mathbf{q}} = \sqrt{\frac{1}{2} \left(\frac{f_{\mathbf{q}}}{\varepsilon_{\mathbf{q}}} - 1 \right)}, \quad (6.16)$$

we can diagonalize H_{MF} and write it as

$$H_{\text{MF}} = \sum_{\mathbf{q}} \varepsilon_{\mathbf{q}} \gamma_{\mathbf{q}}^\dagger \gamma_{\mathbf{q}} + \text{const.}, \quad (6.17)$$

where $g_{\mathbf{q}} = |g_{\mathbf{q}}|e^{i\phi_{\mathbf{q}}}$. The energy eigenvalues are given by

$$\varepsilon_{\mathbf{q}} = \sqrt{f_{\mathbf{q}}^2 - |g_{\mathbf{q}}|^2}. \quad (6.18)$$

An example of the dispersion relation is shown in Fig. 2. Substituting $V = 0$ in the above expressions, the dispersion relation without pinning, $\varepsilon_{\mathbf{q}} \propto |\mathbf{q}|^{3/2}$, is recovered.^{21,28,19}

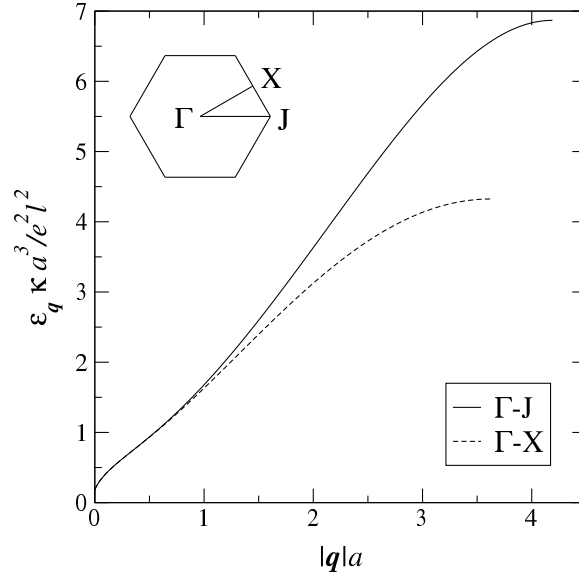


FIG. 2. The dispersion relation of a pinned triangular WC is plotted along two directions within the first Brillouin zone as specified in the inset.

Taylor-expanded in small $|\mathbf{q}|$, the parameters and the energy eigenvalue take the form

$$f_{\mathbf{q}} = (1 - \overline{Q})V + \frac{\nu e^2}{2\kappa} |\mathbf{q}| + \mathcal{O}[|\mathbf{q}|^2], \quad (6.19)$$

$$g_{\mathbf{q}} = \frac{\nu e^2}{2\kappa} \frac{(q_x + i q_y)^2}{|\mathbf{q}|} + \mathcal{O}[|\mathbf{q}|^2], \quad (6.20)$$

$$\varepsilon_{\mathbf{q}} = (1 - \overline{Q})V + \frac{\nu e^2}{2\kappa} |\mathbf{q}| + \mathcal{O}[|\mathbf{q}|^2], \quad (6.21)$$

which are valid if

$$\frac{\nu e^2}{2\kappa} |\mathbf{q}| \ll (1 - \overline{Q})V. \quad (6.22)$$

One of the authors has obtained a similar dispersion relation at $T = 0$.¹⁸ The main difference for this finite temperature model is that the zeroth order term contains the self-consistent MF value \bar{Q} . As pointed out in Ref. 18, the above linear dispersion is a direct consequence of the fact that the Coulomb interaction is long-ranged. With this dispersion relation, the magnetophonon density of states vanishes at the lower band edge, and thermal broadening will be substantially suppressed as will be shown below. This is not the case for a short-range interaction. For example, a screened interaction would have yielded a dispersion that is quadratic at small wave vectors. In that case, the density of states jumps to a finite value at the band edge. In a separate test, we have found that thermal broadening is indeed several orders of magnitude greater for a screened interaction than for an unscreened one.

Since $f_{\mathbf{q}}$ and $\varepsilon_{\mathbf{q}}$ are functions of \bar{Q} , the saddle point solution for \bar{Q} has to be determined self-consistently. More specifically, it has to satisfy

$$\bar{Q} = \frac{1}{N_s} \sum_{\mathbf{q}} \langle b_{l\mathbf{q}}^\dagger b_{l\mathbf{q}} \rangle \quad (6.23)$$

$$= \frac{1}{N_s} \sum_{\mathbf{q}} |u_{\mathbf{q}}|^2 \langle \gamma_{l\mathbf{q}}^\dagger \gamma_{l\mathbf{q}} \rangle + |v_{\mathbf{q}}|^2 \langle \gamma_{l,-\mathbf{q}}^\dagger \gamma_{l,-\mathbf{q}} \rangle \quad (6.24)$$

$$= \frac{1}{N_s} \sum_{\mathbf{q}} \left[\left(n_B(\varepsilon_{\mathbf{q}}) + \frac{1}{2} \right) \frac{f_{\mathbf{q}}}{\varepsilon_{\mathbf{q}}} - \frac{1}{2} \right], \quad (6.25)$$

where $n_B(\varepsilon) = 1/(e^{\beta\varepsilon} - 1)$ is the Bose function.

In the MF theory, the uniform field absorption spectrum will have a delta function peak at $\hbar\omega_p = \varepsilon_{\mathbf{q}=\mathbf{0}}$. Since $\varepsilon_{\mathbf{q}=\mathbf{0}} = V(1 - \bar{Q})$ and \bar{Q} increases with temperature, the thermal reduction of the peak frequency observed in experiments is explained qualitatively already at the MF level. Physical interpretation is also simple. At high temperatures, more magnetophonons are thermally created. This implies that the average number of electrons that stay in the pits decreases, leading to a drop in the spatially averaged pinning potential.

In order to explain thermal broadening, however, one has to go beyond the MF theory. We will compute the first order corrections in the $1/N$ expansion in the next subsection.

B. Order $1/N$ corrections

In this subsection, we will consider fluctuations of the HS field about its MF solution. The fluctuation fields are defined at each site as

$$r_i(\tau) = Q_i(\tau) - \bar{Q} \quad (6.26)$$

and its Fourier-transformed field is

$$r_q = \frac{1}{\beta\sqrt{N_s}} \sum_i e^{-i\mathbf{q}\cdot\mathbf{R}_i} r_i(\tau). \quad (6.27)$$

Since $r_i(\tau)$ is real, $r_{-q} = r_q^*$. In terms of r_q , Eq. (6.4) may be rewritten as

$$\begin{aligned} S_{\text{HS}} = & -\frac{\beta}{2} \sum_l \sum_{qq'} \begin{bmatrix} z_{lq}^* & z_{l,-q} \end{bmatrix} (\mathbf{G}_{\text{MF}}^{-1} + \mathbf{U})_{qq'} \begin{bmatrix} z_{lq'} \\ z_{l,-q'}^* \end{bmatrix} \\ & + \frac{\beta NV}{2} \left(N_s \bar{Q}^2 - 2\sqrt{N_s} \bar{Q} r_{q=0} + \sum_q |r_q|^2 \right), \end{aligned} \quad (6.28)$$

where

$$(\mathbf{G}_{\text{MF}}^{-1})_{qq'} = \begin{bmatrix} i\omega_n - f_{\mathbf{q}} & g_{\mathbf{q}}^* \\ g_{\mathbf{q}} & -i\omega_n - f_{\mathbf{q}} \end{bmatrix} \delta_{qq'}, \quad (6.29)$$

$$\mathbf{U}_{qq'} = -\frac{1}{\sqrt{N_s}} \begin{bmatrix} V r_{q-q'} & 0 \\ 0 & V r_{q+q'} \end{bmatrix}. \quad (6.30)$$

\mathbf{G}_{MF} is the MF magnetophonon Green's function matrix and \mathbf{U} describes the coupling between a magnetophonon and the HS field r , or a vertex in the Feynman diagrams. The “bare” HS propagator can be read off from S_{HS} and is given by

$$D_0 = -\frac{1}{NV}. \quad (6.31)$$

Fig. 3(a) shows the building blocks of the Feynman diagrams that will be frequently used below.

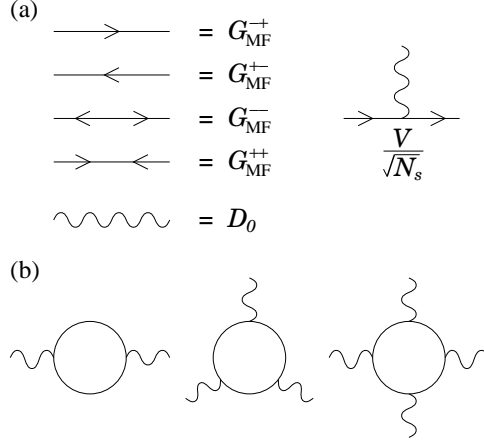


FIG. 3. (a) The Feynman diagrams are drawn for MF magnetophonon Green's functions G_{MF} (straight line), Hubbard-Stratonovich propagator D_0 (curly line), and the vertex $V/\sqrt{N_s}$. The arrows on both sides of a vertex must be the same. Note that there are anomalous Green's functions that have two arrows pointing opposite directions, because the Hamiltonian does not conserve the magnetophonon number. (b) Examples of loops with vertices. Each loop corresponds to a summand of the n -summation in Eq. (6.34). $n = 2, 3$, and 4 respectively. A straight line without arrows denote a sum of all arrowed lines that are permitted by the "direction-conservation" rule at each vertex. The first diagram represents the RPA propagator. Since there is no $n = 1$ term in Eq. (6.34), the Feynman rules do not allow a loop to have only one vertex.

Note that D_0 is proportional to $1/N$, so each curly line raises the order of an overall diagram by one in the $1/N$ expansion. On the other hand, a magnetophonon loop [see Fig. 3(b)] contributes order N due to a summation over an internal species-index. In order to find corrections to the HS propagator, it is convenient to integrate out the magnetophonon degree of freedom. The effective action for the HS field r_q is given by

$$S_{\text{eff}}[r] = -\ln \int \mathcal{D}^2 z e^{-S_{\text{HS}}} \quad (6.32)$$

$$= -\frac{N}{2} \text{tr} \ln [\beta(G_{\text{MF}}^{-1} + \mathbf{U})] + \frac{\beta NV}{2} \left(\sum_q |r_q|^2 - 2\bar{Q}\sqrt{N_s} r_{q=0} \right) \quad (6.33)$$

$$= \frac{N}{2} \left[\text{tr} \ln \frac{G_{\text{MF}}}{\beta} - \sum_{n=2}^{\infty} \frac{1}{n} \text{tr} (G_{\text{MF}} \mathbf{U})^n \right] + \frac{\beta NV}{2} \sum_q |r_q|^2. \quad (6.34)$$

Going from Eq. (6.33) to Eq. (6.34), we have Taylor-series expanded the logarithmic function about βG_{MF}^{-1} . Unimportant constants were omitted at every step. Note that the last term in Eq. (6.33) exactly cancels out the $n = 1$ term that would have been in Eq. (6.34), because \bar{Q} is chosen at a saddle point. G_{MF} and \mathbf{U} are considered as entities in a product space of a 2×2 matrix and a matrix labeled by frequency and wave-number indices qq' . Thus, a trace operator sums not only over the 2×2 matrix indices, but also over q .

Let us take a closer look at the last expression (6.34). The first term is the MF free energy and the last term is the action of free independent HS fields r_q . Each of the remaining terms is represented by a loop with n vertices as in Fig. 3(b).

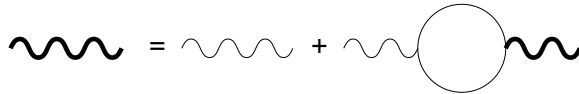


FIG. 4. Dyson equation for the RPA Hubbard-Stratonovich propagator. Thick wiggly lines denote self-consistent solution for the RPA propagator.

Let us now search for the lowest order correction to the HS propagator. There is no correction of the zeroth order or lower, and the only $1/N$ correction comes from the $n = 2$ term of Eq. (6.34). As can be seen in the first Feynman diagram in Fig. 3(b), this term is nothing but the RPA correction to the HS propagator. We explicitly write it as

$$\frac{N}{4} \text{tr} \mathbf{G}_{\text{MF}} \mathbf{U} \mathbf{G}_{\text{MF}} \mathbf{U} = \frac{N\beta V^2}{2} \sum_q \varrho_{\text{MF}}(q) |r_q|^2, \quad (6.35)$$

where $\varrho_{\text{MF}}(q)$ is the MF magnetophonon density-density correlation function defined as

$$\varrho_{\text{MF}}(q) = \frac{1}{2\beta N_s} \sum_{q'} \text{tr} \mathbf{G}_{\text{MF}}(q' - q) \mathbf{G}_{\text{MF}}(q') \quad (6.36)$$

$$= \int d\tau e^{i\omega_n \tau - i\mathbf{q} \cdot \mathbf{R}_i} \left\langle b_i^\dagger b_i(\tau) b_0^\dagger b_0(0) \right\rangle_{\text{MF}}, \quad (6.37)$$

where $\langle \dots \rangle_{\text{MF}}$ denotes an average in the MF theory. Detailed calculations of $\varrho_{\text{MF}}(q)$ will be given in Appendix A. The RPA “dressed” propagator is defined through the Dyson equation

$$D(q) = \frac{1}{D_0^{-1} + NV^2 \varrho_{\text{MF}}(q)} \quad (6.38)$$

$$= -\frac{1}{NV(1 - V \varrho_{\text{MF}}(q))}. \quad (6.39)$$

Since both the bare propagator D_0 and the RPA correction are of order $1/N$, the above propagator is also of order $1/N$. A thick curly line will be used for the Feynman diagram of the dressed propagator as in Fig. 4.

$$\begin{aligned} \Sigma_I^{\sigma\rho}(q) &= \Sigma_a^{\sigma\rho}(q) + \Sigma_b \delta_{\sigma\rho} \\ &= \text{diagram 1} + \text{diagram 2} \times \delta_{\sigma\rho} \end{aligned}$$

FIG. 5. Two self-energy diagrams of order $1/N$. The indices σ and ρ take either $+$ or $-$. They also determine the direction of arrows in the diagram of Σ_a . A $-$ ($+$) sign means annihilation (creation) of a magnetophonon, so the corresponding arrow points towards (away from) the nearby vertex.

We now have all the ingredients to calculate the $1/N$ correction to the magnetophonon Green’s function. Keeping in mind that each HS propagator is of order $1/N$ and each magnetophonon loop is of order N , it is straightforward to count the order of any Feynman diagram. There are two self-energy diagrams of order $1/N$ as shown in Fig. 5. They are written in terms of MF Green’s functions $G_{\text{MF}}^{\sigma\rho}$ and the HS propagator D as

$$\Sigma_a^{\sigma\rho}(q) = -\frac{V^2}{\beta N_s} \sum_{q'} D(q - q') G_{\text{MF}}^{\sigma\rho}(q'), \quad (6.40)$$

$$\begin{aligned} \Sigma_b &= \frac{NV^4}{\beta^2 N_s^2} D(0) \sum_{q'q''} D(-q' - q'') \\ &\times \left\{ G_{\text{MF}}^{-+}(q'') \left[(G_{\text{MF}}^{-+}(q'))^2 + G_{\text{MF}}^{--}(q') G_{\text{MF}}^{++}(q') \right] \right. \\ &\left. + \left[G_{\text{MF}}^{--}(q'') G_{\text{MF}}^{++}(q') G_{\text{MF}}^{-+}(q') + \text{c.c.} \right] \right\}. \end{aligned} \quad (6.41)$$

These expressions can be partially evaluated analytically via frequency summations.³³ More details may be found in Appendix B.

The self-energy correction is incorporated into the Green’s functions via the Dyson equation

$$\mathbf{G}(q) = [\mathbf{G}_{\text{MF}}^{-1}(q) - \Sigma_a(q) - \mathbf{I}\Sigma_b]^{-1}, \quad (6.42)$$

where

$$\Sigma_a = \begin{bmatrix} \Sigma_a^{--} & \Sigma_a^{+-} \\ \Sigma_a^{+-} & \Sigma_a^{++} \end{bmatrix}, \quad \mathbf{l} = \begin{bmatrix} 1 & 0 \\ 0 & 1 \end{bmatrix}. \quad (6.43)$$

Combining Eq. (6.42) with Eqs. (3.5), (3.7), and (3.8), we can finally compute the ac conductivity to the order $1/N$. Using the final expressions in Appendix B, we have numerically computed the self-energy diagrams and obtained the conductivity as a function of T . The result is presented in the next section.

VII. RESULT

Before we present the result, it is useful to review some important energy scales. For the purpose of comparison, we will use the data in Ref. 8. We find

$$\begin{aligned} \frac{e^2}{\kappa l_0} &\gtrsim 16 \text{ meV}, \\ \hbar\omega_c &\gtrsim 3 \text{ meV}, \\ \frac{e^2}{\kappa a} &\sim 2 \text{ meV}, \\ \frac{e^2 l_0^2}{\kappa a^3} &\lesssim 60 \text{ } \mu\text{eV}, \\ \hbar\omega_p &\sim 5 \text{ } \mu\text{eV}. \end{aligned} \quad (7.1)$$

The temperature range for which the line width was clearly discernible was $3 \text{ } \mu\text{eV} \leq k_B T \lesssim 18 \text{ } \mu\text{eV}$.

For efficiency in numerical computations, we have made the following isotropic approximations

$$\begin{aligned} f_{\mathbf{q}} &= f(|\mathbf{q}|), \\ g_{\mathbf{q}} &= g(|\mathbf{q}|) \left(\frac{q_x + iq_y}{|\mathbf{q}|} \right)^2, \\ \varepsilon_{\mathbf{q}} &= \varepsilon(|\mathbf{q}|). \end{aligned} \quad (7.2)$$

We did, however, keep the shape of the first Brillouin zone to be hexagonal. According to our numerical tests, these approximations break down as the Brillouin zone boundaries are approached, i.e., when $|\mathbf{q}| \sim \pi/a$, but they are very accurate for $|\mathbf{q}| \lesssim 1/a$. For example, when $V \sim \hbar\omega_p$, the energy $\varepsilon_{\mathbf{q}}$ is already an order of magnitude greater than $\hbar\omega_p$ at $|\mathbf{q}| = 1/a$ (see Fig. 2), but the error $\Delta\varepsilon$ is still less than 4%. Therefore, this approximation should be quantitatively reliable if T is not too much greater than $\hbar\omega_p$.

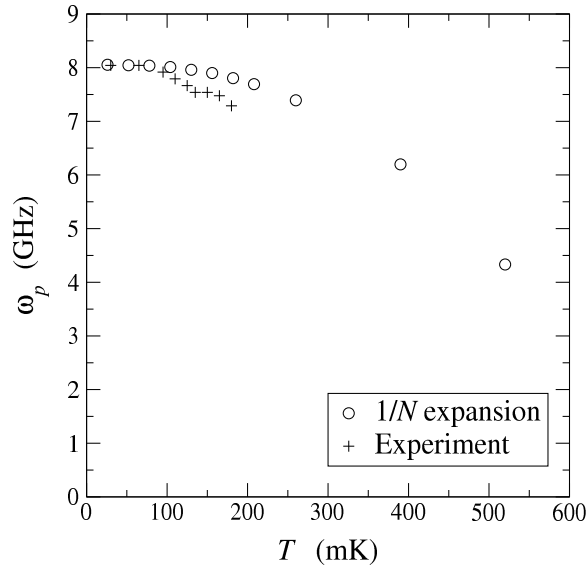


FIG. 6. Peak frequency as a function of temperature. Our results are overestimated compared to the experimental data (Ref. 8), but there is a good qualitative agreement.

In order to compare our result with the experimental data, we have chosen the bare pinning potential V in such a way that the resulting peak frequency ω_p agrees with the experiment at the lowest measured temperature. The peak position data are shown in Fig. 6, along with experimental data from Ref. 8. Although our results are systematically overestimated, the qualitative agreement is rather good.

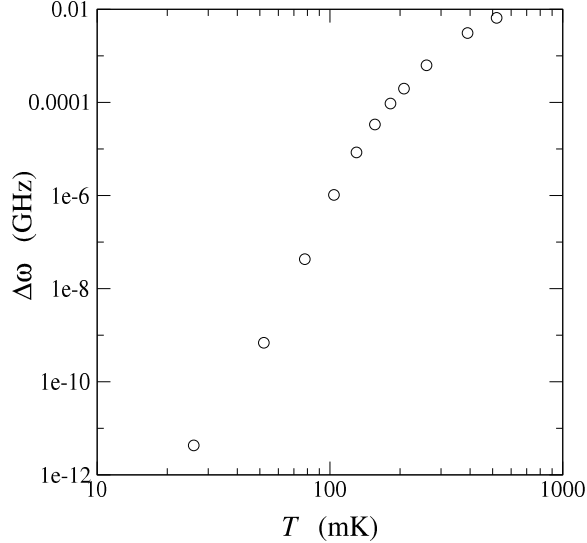


FIG. 7. The half-width-half-maximum line width is plotted against temperature in log-log scale. The peaks appear to be extremely sharp especially in the low temperature regime. However, the width increases very rapidly with temperature.

The results for line width $\Delta\omega$ are surprisingly small (Fig. 7). Compared to those from experimental data, our results are several orders of magnitude smaller at the lowest T . This is especially surprising because $T \sim \hbar\omega_p$. Naïvely, one would expect that the line width should be of the same order of magnitude as T , due to thermal broadening. Although much greater than our results, experiments also confirm that this is clearly not the case. In Refs. 7 and 8, $\Delta\omega$ is almost one order of magnitude smaller than ω_p . In Ref. 9, the quality factor $Q = \omega_p/\Delta\omega$ even exceeds 30. There are also other indications that the peaks may be actually even sharper.³⁴

The unusually sharp peak may be rather well understood within our model. As discussed in Sec. VI A, due to the long-range Coulomb interaction, the dispersion starts out linearly in $|\mathbf{q}|$. The density of states thus increases linearly from zero. Explicitly, the density of states per unit cell takes the form

$$\mathcal{N}(\varepsilon) = \begin{cases} \frac{1}{2\pi} \left(\frac{2\kappa}{\nu e^2} \right)^2 [\varepsilon - (1 - \bar{Q})V] & \text{if } \varepsilon > (1 - \bar{Q})V, \\ 0 & \text{if } \varepsilon \leq (1 - \bar{Q})V. \end{cases} \quad (7.3)$$

A rough estimate of the total number of “accessible states” per site at temperature T would be

$$\sim a_c \int_0^T d\varepsilon \mathcal{N}(\varepsilon), \quad (7.4)$$

where a_c is the unit cell area. Using the parameters in Ref. 8, we find that there are merely 2×10^{-4} accessible states per site at $T = 180$ mK, which is the highest temperature for which the line width was measured. The physical interpretation of this may be given as the following. At least in the semiclassical level, our model is essentially that of a crystal in which each electron is attached to a lattice site by a short-range binding potential. The overall uniform motion ($\mathbf{q} = \mathbf{0}$) determines the peak frequency. Broadening comes about from thermal and quantum fluctuations deforming the lattice and making the electrons move relative to one another. However, the above analysis tells us that a WC in a strong magnetic field is so rigid that it is hardly deformed even at temperatures greater than the pinning potential.

In reality, the external ac field has a finite wave length of order $\sim 30 \mu\text{m} \sim 10^5 a$ (Ref. 7). Accordingly, we have performed a similar analysis for the response at the finite wave vector, but we found no qualitative change.

Defects in a WC such as interstitials, vacancies, dislocations, etc. may also affect broadening. It is certainly true that their presence will soften the lattice and subsequently enhance magnetophonon excitations. However, unless one is too close to the melting temperature of the WC, which is not the case in the experiments, their effects may be

mostly taken into account through renormalization of the lattice stiffness, or dynamic matrix in Eq. (4.5). This should not affect our results qualitatively.

There may be other sources of broadening, too. Other low energy modes, which are not included in this work, may be involved in the broadening. One possible candidate is the edge states of the WC,³⁵ the analysis of which will be given elsewhere. Another possible source of broadening is extrinsic low energy modes *outside* the WC. When an experiment is performed, there are many external degrees of freedom that may be coupled to the sample. If some of them are hard to remove and thus are left undetected to influence the data, the observed peak will be certainly broader than theoretically predicted.

It has also been suggested that higher Landau level mixing might be important.³⁶ It is certainly true that there can be second or higher order scattering processes that use higher Landau levels as virtual states. However, these processes should be suppressed as a power $(\omega_p/\omega_c)^a$ with $a \geq 1$. Since $\omega_p/\omega_c \sim 10^{-3}$, $\Delta\omega$ as a result of such processes would be still too small to explain currently available experimental data.

VIII. CONCLUSION

In this work, we studied the thermal broadening of the electromagnetic absorption resonance of a magnetically induced WC. In the strong magnetic field limit, the low-energy collective modes that are coupled to the spatially uniform ac electric field are magnetophonons. Assuming that electrons are closely bound to lattice sites, magnetophonon creation and annihilation operators may be constructed out of displacements $\mathbf{u}_i = \mathbf{r}_i - \mathbf{R}_i$.

We showed that the Hamiltonian could be divided into harmonic and anharmonic parts in terms of magnetophonon operators. The harmonic part, when taken alone, describes independent magnetophonons and produces a delta function peak in the spectrum. The anharmonic part introduces magnetophonon interactions. It will not only renormalize the peak position, but also broaden it by mixing different magnetophonon modes. Anharmonicity in our model comes from two sources: the Coulomb interaction and the pinning potential. Since the Coulomb interaction depends only on the relative coordinates, it is completely decoupled from the center-of-mass degrees of freedom. This leads to the derivation of a generalized Kohn's theorem that asserts that the Coulomb interaction cannot shift or broaden an ac conductivity resonance peak even in the presence of a uniform harmonic pinning potential.

Analysis of the magnetophonon interactions in the pinning potential was performed using a $1/N$ expansion technique. This technique provides a systematic way of summing up important diagrams and it captures important pieces of physics in the low order solutions. For example, we found that the zeroth order MF solution could account for the decreasing peak frequency ω_p as a function of temperature.

Thermal broadening appears in the $1/N$ self-energy corrections. However, the line width $\Delta\omega$ is found to be many orders of magnitude smaller than ω_p and T . The reason for this lies in the magnetophonon dispersion that is linear and steep in the low energy limit. This translates into a small density of states for collective excitations. Consequently the broadening is substantially suppressed.

Our result of peak frequency agrees qualitatively with recent experiments.^{7,8} The line width result is also qualitatively consistent in that it is much less than ω_p and T . Quantitatively, our result of $\Delta\omega$ appears to be much smaller than published results, although there is continuing experimental work on sorting out just how narrow the intrinsic line width really is.³⁴ Other possible sources of broadening, such as edge states and extrinsic low energy modes, may also be responsible for observed line width.

ACKNOWLEDGMENT

We are indebted to Lloyd Engel, Chi-Chun Li, Dan Tsui, and Jongsoo Yoon for helpful discussions regarding their experiments. Carsten Timm and Steve Girvin are gratefully acknowledged for useful discussions about the $1/N$ expansion technique. We also thank Institute for Theoretical Physics, UC Santa Barbara, where part of this work was done. This work was supported by NSF Grant DMR98-70681 and PHY94-07194 and the Research Corporation.

APPENDIX A: DENSITY-DENSITY CORRELATION $\varrho_{\text{MF}}(q)$

In this Appendix, we will present detailed calculations of the density-density correlation function $\varrho_{\text{MF}}(q)$. Eq. (6.36) can be written as

$$\begin{aligned}
\varrho_{\text{MF}}(q) &= \frac{1}{2\beta N_s} \sum_{q'} [G_{\text{MF}}^{--}(q' - q)G_{\text{MF}}^{--}(q') + G_{\text{MF}}^{--}(q' - q)G_{\text{MF}}^{++}(q') + G_{\text{MF}}^{++}(q' - q)G_{\text{MF}}^{--}(q') + G_{\text{MF}}^{++}(q' - q)G_{\text{MF}}^{++}(q')] \\
&= \frac{1}{\beta N_s} \sum_{q'} [G_{\text{MF}}^{--}(q' - q)G_{\text{MF}}^{--}(q') + G_{\text{MF}}^{--}(q' - q)G_{\text{MF}}^{++}(q'),]
\end{aligned} \tag{A1}$$

where we have used

$$G_{\text{MF}}^{\sigma\rho}(-q) = G_{\text{MF}}^{\rho\sigma}(q) \tag{A2}$$

to get the second line. Diagrammatically, the last two terms are represented by two arrowed diagrams as in Fig. 8.

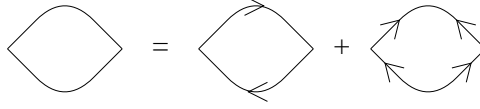


FIG. 8. Two arrowed diagrams for the density-density correlation function $\varrho_{\text{MF}}(q)$.

Using the Green's functions in Eq. (6.9), we may rewrite the above equation more explicitly as

$$\varrho_{\text{MF}}(q) = \frac{1}{\beta N_s} \sum_{q'} \frac{2(i\omega'_n - i\omega_n)i\omega'_n + 2f_{\mathbf{q}'-\mathbf{q}}f_{\mathbf{q}'} + g_{\mathbf{q}'-\mathbf{q}}^*g_{\mathbf{q}'} + g_{\mathbf{q}'-\mathbf{q}}g_{\mathbf{q}'}^*}{2[(i\omega'_n - i\omega_n)^2 - \varepsilon_{\mathbf{q}'-\mathbf{q}}^2][(i\omega'_n)^2 - \varepsilon_{\mathbf{q}'}^2]} \tag{A3}$$

$$= \frac{1}{2N_s} \sum_{\mathbf{q}'} \left[(n_{\mathbf{q}'-\mathbf{q}} - n_{\mathbf{q}'}) \frac{(\varepsilon_{\mathbf{q}'-\mathbf{q}} - \varepsilon_{\mathbf{q}'}) (1 + \xi_{\mathbf{q}'-\mathbf{q},\mathbf{q}'})}{(i\omega_n)^2 - (\varepsilon_{\mathbf{q}'-\mathbf{q}} - \varepsilon_{\mathbf{q}'})^2} + (n_{\mathbf{q}'-\mathbf{q}} + n_{\mathbf{q}'} + 1) \frac{(\varepsilon_{\mathbf{q}'-\mathbf{q}} + \varepsilon_{\mathbf{q}'}) (1 - \xi_{\mathbf{q}'-\mathbf{q},\mathbf{q}'})}{(i\omega_n)^2 - (\varepsilon_{\mathbf{q}'-\mathbf{q}} + \varepsilon_{\mathbf{q}'})^2} \right], \tag{A4}$$

where $n_{\mathbf{q}'}$ is a shorthand notation of the Bose function $n_B(\varepsilon_{\mathbf{q}'})$. In the second line, we have used the usual frequency summation technique.³³

$\varrho(q)$ has many simple poles in the complex ω plane on the real axis. In the thermodynamic limit, they become branch cuts. Therefore, summations involving $\varrho(q)$ must be performed with care, as will be demonstrated in the calculations of self energy corrections in the next Appendix. Note that $\varrho(q)$ is analytic and real at $\omega = 0$, so that the branch cuts are divided into two: one on the positive and the other on the negative axis. Both branch cuts are bounded because $\varepsilon_{\mathbf{q}'-\mathbf{q}} \pm \varepsilon_{\mathbf{q}'}$ is finite.

Eventually, we will analytically continue $i\omega_n \rightarrow \omega + i0^+$ to get a retarded correlation function. Since $\varrho(-q) = \varrho(q)$ and $\varrho(q)$ is analytic except on the branch cuts, it has the following properties:

$$\begin{aligned}
\text{Re } \varrho(-\omega + i0^+, \mathbf{q}) &= \text{Re } \varrho(\omega + i0^+, \mathbf{q}), \\
\text{Im } \varrho(-\omega + i0^+, \mathbf{q}) &= -\text{Im } \varrho(\omega + i0^+, \mathbf{q}),
\end{aligned} \tag{A5}$$

which will become useful in the next Appendix. Finally, $\varrho(\omega + i0^+, \mathbf{q})$ was numerically computed using an isotropic approximation as explained in Sec. VII.

APPENDIX B: $1/N$ SELF ENERGY CORRECTIONS $\Sigma_A^{\sigma\rho}$ AND Σ_B

In this Appendix, we will calculate the $1/N$ self energy corrections to the magnetophonon Green's functions as in Fig. 5. Since the bare HS propagator D_0 is a constant, it is convenient to separate it from the rest of the RPA dressed propagator D . The remaining part

$$\delta D(\mathbf{q}) \equiv D(\mathbf{q}) - D_0 \tag{B1}$$

$$= \frac{\varrho_0(\mathbf{q})}{N[V\varrho_0(\mathbf{q}) - 1]} \tag{B2}$$

vanishes as ω^{-2} in the large ω limit, so all following frequency sums that contain $\delta D(\mathbf{q})$ converge without introducing cumbersome convergence factors such as $e^{\pm i\omega 0^+}$.

The first self-energy correction $\Sigma_a^{\sigma\rho}(q)$ is given in Eq. (6.40). The contribution of the bare propagator D_0 is simply

$$\Sigma_{a0}^{\sigma\rho} = -\frac{V^2}{\beta N_s} D_0 \sum_{q'} G_{\text{MF}}^{\sigma\rho}(q'). \tag{B3}$$

The summation of MF Green's function is defined with an appropriate convergence factor that ensures normal-ordering. It is then straightforward to show

$$\sum_{q'} G_{\text{MF}}^{-+}(q') = -\beta \sum_{\mathbf{q}'} \langle b_{\mathbf{q}'}^\dagger b_{\mathbf{q}'} \rangle = -\beta N_s n_{\text{ph}}, \quad (\text{B4})$$

$$\sum_{q'} G_{\text{MF}}^{+-}(q') = -\beta N_s n_{\text{ph}}, \quad (\text{B5})$$

$$\sum_{q'} G_{\text{MF}}^{--}(q') = -\beta \sum_{\mathbf{q}'} \langle b_{\mathbf{q}'} b_{\mathbf{q}'} \rangle \equiv -\beta N_s n_{\text{an}}, \quad (\text{B6})$$

$$\sum_{q'} G_{\text{MF}}^{--}(q') = -\beta \sum_{\mathbf{q}'} \langle b_{\mathbf{q}'}^\dagger b_{\mathbf{q}'}^\dagger \rangle = -\beta N_s n_{\text{an}}^*, \quad (\text{B7})$$

where n_{an} is the anomalous magnetophonon number per site. Due to the six-fold symmetry of the lattice, however, $n_{\text{an}} = 0$. We therefore get

$$\begin{aligned} \Sigma_{a0}^{-+} &= \Sigma_{a0}^{+-} = -\frac{n_{\text{ph}} V}{N}, \\ \Sigma_{a0}^{--} &= \Sigma_{a0}^{++} = 0. \end{aligned} \quad (\text{B8})$$

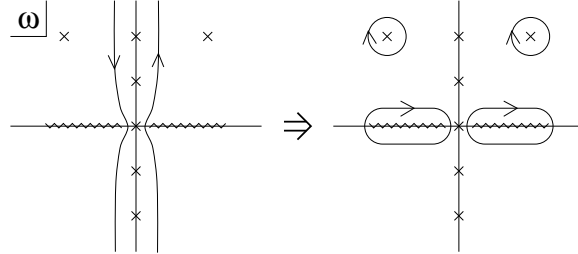


FIG. 9. Contour is deformed in the complex ω . Simple poles are denoted by \times and branch cuts by zigzag lines. The separation between two branch cuts is exaggerated in order to show that the pole at the origin is treated separately. In fact, the branch cuts asymptotically touch the origin.

Now let us turn our attention to the remaining part. It needs to be computed with more care, since $\delta D(q')$ has branch cuts on the real ω axis, that arise from the density-density correlation function $\varrho(q')$. Using the Green's functions in Eq. (6.9), we may write

$$\delta \Sigma_a^{-+}(q) = -\frac{V^2}{N\beta N_s} \sum_{q'} \delta D(q - q') G_{\text{MF}}^{-+}(q') \quad (\text{B9})$$

$$= -\frac{V^2}{N\beta N_s} \sum_{q'} \delta D(q - q') \left[\frac{|u_{\mathbf{q}'}|^2}{i\omega_n' - \varepsilon_{\mathbf{q}'}} - \frac{|v_{\mathbf{q}'}|^2}{i\omega_n' + \varepsilon_{\mathbf{q}'}} \right], \quad (\text{B10})$$

where $u_{\mathbf{q}'}$ and $v_{\mathbf{q}'}$ are defined in Eqs. (6.15) and (6.16). As in a standard frequency summation technique,³³ we may replace the sum over $i\omega_n'$ by a contour integral on the complex ω' plane with simple poles on the imaginary axis. After the contour is deformed as in Fig. 9, the new expression takes the form

$$\begin{aligned} \delta \Sigma_a^{-+}(q) &= \frac{V^2}{N N_s} \sum_{\mathbf{q}'} [\delta D(i\omega_n - \varepsilon_{\mathbf{q}'}, \mathbf{q} - \mathbf{q}') |u_{\mathbf{q}'}|^2 + \delta D(i\omega_n + \varepsilon_{\mathbf{q}'}, \mathbf{q} - \mathbf{q}') |v_{\mathbf{q}'}|^2] n_B(\varepsilon_{\mathbf{q}'}) \\ &\quad - \frac{V^2}{\pi N N_s} \sum_{\mathbf{q}'} \int_{\omega' \neq 0} d\omega' [\text{Im } \delta D(\omega' + i0^+, \mathbf{q} - \mathbf{q}')] \left[\frac{|u_{\mathbf{q}'}|^2 n_B(\omega')}{i\omega_n + \omega' - \varepsilon_{\mathbf{q}'}} + \frac{|v_{\mathbf{q}'}|^2 n_B(-\omega')}{i\omega_n + \omega' + \varepsilon_{\mathbf{q}'}} \right], \end{aligned} \quad (\text{B11})$$

where $\omega' = 0$ is excluded from the domain of the integral

$$\int_{\omega' \neq 0} = \int_{-\infty}^{0^-} + \int_{0^+}^{\infty}. \quad (\text{B12})$$

Although $n_B(\omega')$ diverges as $\omega' \rightarrow 0$, the above integral is well defined, because $\text{Im } \delta D(\omega' + i0^+, \mathbf{q} - \mathbf{q}')$ vanishes as $\omega' = 0$ is approached. Finally, analytic continuation is performed to give

$$\begin{aligned} \delta \Sigma_a^{-+}(\omega + i0^+, \mathbf{q}) &= \frac{V^2}{NN_s} \sum_{\mathbf{q}'} [\delta D(\omega - \varepsilon_{\mathbf{q}'} + i0^+, \mathbf{q} - \mathbf{q}') |u_{\mathbf{q}'}|^2 + \delta D(\omega + \varepsilon_{\mathbf{q}'} + i0^+, \mathbf{q} - \mathbf{q}') |v_{\mathbf{q}'}|^2] n_B(\varepsilon_{\mathbf{q}'}) \\ &\quad - \frac{V^2}{\pi NN_s} \sum_{\mathbf{q}'} P \int d\omega' \text{Im } \delta D(\omega' + i0^+, \mathbf{q} - \mathbf{q}') \left[\frac{|u_{\mathbf{q}'}|^2 n_B(\omega')}{\omega + \omega' - \varepsilon_{\mathbf{q}'}} + \frac{|v_{\mathbf{q}'}|^2 n_B(-\omega')}{\omega + \omega' + \varepsilon_{\mathbf{q}'}} \right] \\ &\quad - i \frac{V^2}{NN_s} \sum_{\mathbf{q}'} \left[\text{Im } \delta D(\omega - \varepsilon_{\mathbf{q}'} + i0^+, \mathbf{q} - \mathbf{q}') |u_{\mathbf{q}'}|^2 n_B(\varepsilon_{\mathbf{q}'} - \omega) \right. \\ &\quad \left. + \text{Im } \delta D(\omega + \varepsilon_{\mathbf{q}'} + i0^+, \mathbf{q} - \mathbf{q}') |v_{\mathbf{q}'}|^2 n_B(\varepsilon_{\mathbf{q}'} + \omega) \right], \end{aligned} \quad (\text{B13})$$

where $P \int$ denotes a Cauchy principal integral. Eq. (A5) was used in the last line. The above quantity may be computed using the numerical solution of $\varrho(\omega + i0^+, \mathbf{q})$. The other $\delta \Sigma_a$'s can be calculated in a similar way. The final form of $\delta \Sigma_a^{+-}$ is the same the above equation, except that $|u_{\mathbf{q}'}|^2$ and $|v_{\mathbf{q}'}|^2$ are switched. $\delta \Sigma_a^{--}$ ($\delta \Sigma_a^{++}$) is obtained by replacing both $|u_{\mathbf{q}'}|^2$ and $|v_{\mathbf{q}'}|^2$ by $u_{\mathbf{q}'}^* v_{\mathbf{q}'}$ ($u_{\mathbf{q}'} v_{\mathbf{q}'}^*$). In the isotropic approximation, the angular sum of

$$u_{\mathbf{q}'}^* v_{\mathbf{q}'} = \frac{g_{\mathbf{q}'}}{2\varepsilon_{\mathbf{q}'}} \propto q_x - iq_y \quad (\text{B14})$$

vanishes, so

$$\delta \Sigma_a^{--} = \delta \Sigma_a^{++} = 0. \quad (\text{B15})$$

The other $1/N$ correction, Σ_b , may be calculated in a similar manner. First, we compute the contribution from the bare HS propagator. Substituting D_0 for $D(-q' - q'')$, Eq. (6.41) becomes

$$\Sigma_{b0} = -\frac{V^3}{\beta^2 N_s^2} D(0) \sum_{q'q''} \left\{ G_{\text{MF}}^{-+}(q'') \left[(G_{\text{MF}}^{-+}(q'))^2 + G_{\text{MF}}^{--}(q) G_{\text{MF}}^{++}(q') \right] + \left[G_{\text{MF}}^{--}(q'') G_{\text{MF}}^{++}(q') G_{\text{MF}}^{-+}(q') + \text{c.c.} \right] \right\}. \quad (\text{B16})$$

Using Eqs. (B4) through (B7) along with

$$\begin{aligned} \sum_{q'} (G_{\text{MF}}^{-+}(q'))^2 &= \sum_{q'} \left(\frac{|u_{\mathbf{q}'}|^2}{i\omega_n - \varepsilon_{\mathbf{q}'}} - \frac{|v_{\mathbf{q}'}|^2}{i\omega_n + \varepsilon_{\mathbf{q}'}} \right)^2 \\ &= -\beta \sum_{\mathbf{q}'} \left[(|u_{\mathbf{q}'}|^4 + |v_{\mathbf{q}'}|^4) n'_B(\varepsilon_{\mathbf{q}'}) - 2|u_{\mathbf{q}'}|^2 |v_{\mathbf{q}'}|^2 \frac{2n_B(\varepsilon_{\mathbf{q}'} + 1)}{2\varepsilon_{\mathbf{q}'}} \right], \end{aligned} \quad (\text{B17})$$

$$\begin{aligned} \sum_{q'} G_{\text{MF}}^{--}(q') G_{\text{MF}}^{++}(q') &= \sum_{q'} |u_{\mathbf{q}'}|^2 |v_{\mathbf{q}'}|^2 \left(\frac{1}{i\omega_n - \varepsilon_{\mathbf{q}'}} - \frac{1}{i\omega_n + \varepsilon_{\mathbf{q}'}} \right)^2 \\ &= -\beta \sum_{\mathbf{q}'} |u_{\mathbf{q}'}|^2 |v_{\mathbf{q}'}|^2 \left[n'_B(\varepsilon_{\mathbf{q}'}) - \frac{2n_B(\varepsilon_{\mathbf{q}'} + 1)}{2\varepsilon_{\mathbf{q}'}} \right], \end{aligned} \quad (\text{B18})$$

we get

$$\Sigma_{b0} = \frac{V^2 n_{\text{ph}}}{[V \varrho(0) - 1] NN_s} \sum_{\mathbf{q}'} \left\{ \frac{|g_{\mathbf{q}'}|^2}{\varepsilon_{\mathbf{q}'}} \frac{2n_B(\varepsilon_{\mathbf{q}'} + 1)}{2\varepsilon_{\mathbf{q}'}} - \frac{f_{\mathbf{q}'}^2}{\varepsilon_{\mathbf{q}'}} n'_B(\varepsilon_{\mathbf{q}'}) \right\}. \quad (\text{B19})$$

The derivative of the Bose function satisfies $n'_B(\varepsilon_{\mathbf{q}'}) = -\beta n_B(\varepsilon_{\mathbf{q}'}) [n_B(\varepsilon_{\mathbf{q}'} + 1)]$.

For the remaining part, we substitute $\delta D(-q' - q'')$ for $D(-q' - q'')$. We get

$$\begin{aligned} \delta \Sigma_b &= \frac{NV^4}{\beta^2 N_s^2} D(0) \sum_{q'q''} \frac{\delta D(-q' - q'')}{i\omega_n'' - \varepsilon''} \left[\frac{|u' u''^* + v' v''^*|^2 (|u'|^2 + |v'|^2)}{(i\omega_n' + \varepsilon')^2} + \frac{|u' v'' + v' u''|^2 (|u'|^2 + |v'|^2)}{(i\omega_n' - \varepsilon')^2} \right. \\ &\quad \left. - \frac{2(u' u''^* + v' v''^*)(u' v'' + v' u'') u'^* v'^* + \text{c.c.}}{(i\omega_n')^2 - \varepsilon'^2} \right]. \end{aligned} \quad (\text{B20})$$

Shorthand notations are defined as $u' \equiv u_{\mathbf{q}'}$, $u'' \equiv u_{\mathbf{q}''}$, etc. In order to avoid the branch cuts in δD , we make a change of variables $i\omega'_n \rightarrow -i\omega'_n - i\omega''_n$ and perform the frequency sum over $i\omega''_n$. The result takes the form

$$\begin{aligned} \delta\Sigma_b = & -\frac{NV^4}{\beta N_s^2} D(0) \sum_{\mathbf{q}'\mathbf{q}''} \delta D(i\omega'_n, -\mathbf{q}' - \mathbf{q}'') \left\{ |u'u''^* + v'v''^*|^2 (|u'|^2 + |v'|^2) \left[\frac{n_B(\varepsilon'') - n_B(\varepsilon')}{(i\omega'_n - \varepsilon' + \varepsilon'')^2} - \frac{n'_B(\varepsilon')}{i\omega'_n - \varepsilon' + \varepsilon''} \right] \right. \\ & + |u'v'' + v'u''|^2 (|u'|^2 + |v'|^2) \left[\frac{n_B(\varepsilon'') + n_B(\varepsilon') + 1}{(i\omega'_n + \varepsilon' + \varepsilon'')^2} - \frac{n'_B(\varepsilon')}{i\omega'_n + \varepsilon' + \varepsilon''} \right] \\ & \left. - \frac{(u'u''^* + v'v''^*)(u'v'' + v'u'')u'^*v'^* + \text{c.c.}}{\varepsilon'} \left[\frac{n_B(\varepsilon'') - n_B(\varepsilon')}{i\omega'_n - \varepsilon' + \varepsilon''} - \frac{n_B(\varepsilon'') + n_B(\varepsilon') + 1}{i\omega'_n + \varepsilon' + \varepsilon''} \right] \right\}. \quad (\text{B21}) \end{aligned}$$

The last frequency sum $\sum_{i\omega'_n}$ is performed using a similar contour deformation technique as in Fig. 9. Using

$$\sum_{i\omega'_n} \frac{\delta D(i\omega'_n)}{i\omega'_n - \varepsilon} = \frac{\beta}{\pi} \text{Im} \int_{\omega' \neq 0} d\omega' \frac{\delta D(\omega' + i0^+) n_B(\omega')}{\omega' - \varepsilon + i0^+} \quad (\text{B22})$$

$$= \frac{\beta}{\pi} P \int d\omega' \frac{\text{Im} \delta D(\omega' + i0^+) n_B(\omega')}{\omega' - \varepsilon} - \beta \text{Re} \delta D(\varepsilon + i0^+) n_B(\varepsilon), \quad (\text{B23})$$

$$\sum_{i\omega'_n} \frac{\delta D(i\omega'_n)}{(i\omega'_n - \varepsilon)^2} = \frac{\beta}{\pi} \text{Im} \int_{\omega' \neq 0} d\omega' \left[\frac{\partial}{\partial \omega'} \delta D(\omega' + i0^+) n_B(\omega') \right] \frac{1}{\omega' - \varepsilon + i0^+}, \quad (\text{B24})$$

Eq. (B21) becomes

$$\begin{aligned} \delta\Sigma_b = & -\frac{V^3}{[V\varrho(0) - 1]N_s^2} \sum_{\mathbf{q}'\mathbf{q}''} \text{Im} \int_{\omega' \neq 0} d\omega' \left\{ \delta D(\omega', -\mathbf{q}' - \mathbf{q}'') n_B(\omega') \left(\frac{c_1}{\omega' - \varepsilon' + \varepsilon'' + i0^+} + \frac{c_2}{\omega' + \varepsilon' + \varepsilon'' + i0^+} \right) \right. \\ & \left. + \left[\frac{\partial}{\partial \omega'} \delta D(\omega', -\mathbf{q}' - \mathbf{q}'') n_B(\omega') \right] \left(\frac{c_3}{\omega' - \varepsilon' + \varepsilon'' + i0^+} + \frac{c_4}{\omega' + \varepsilon' + \varepsilon'' + i0^+} \right) \right\}, \quad (\text{B25}) \end{aligned}$$

where

$$c_1 = -|u'u''^* + v'v''^*|^2 (|u'|^2 + |v'|^2) n'_B(\varepsilon') + \frac{(u'u''^* + v'v''^*)(u'v'' + v'u'')u'^*v'^* + \text{c.c.}}{\varepsilon'} [n_B(\varepsilon') - n_B(\varepsilon'')], \quad (\text{B26})$$

$$c_2 = -|u'v'' + v'u''|^2 (|u'|^2 + |v'|^2) n'_B(\varepsilon') + \frac{(u'u''^* + v'v''^*)(u'v'' + v'u'')u'^*v'^* + \text{c.c.}}{\varepsilon'} [n_B(\varepsilon') + n_B(\varepsilon'') + 1], \quad (\text{B27})$$

$$c_3 = -|u'u''^* + v'v''^*|^2 (|u'|^2 + |v'|^2) [n_B(\varepsilon') - n_B(\varepsilon'')], \quad (\text{B28})$$

$$c_4 = |u'v'' + v'u''|^2 (|u'|^2 + |v'|^2) [n_B(\varepsilon') + n_B(\varepsilon'') + 1]. \quad (\text{B29})$$

Finally, combining Eqs. (B8), (B13), (B19), and (B25), the order $1/N$ self-energy correction is given by

$$\Sigma_1^{\sigma\rho} = \Sigma_{a0}^{\sigma\rho} + \delta\Sigma_a^{\sigma\rho} + (\Sigma_{b0} + \delta\Sigma_b)\delta\sigma_\rho. \quad (\text{B30})$$

¹ E. P. Wigner, Phys. Rev. **46**, 1002 (1934).

² For more discussion on the subject, see, for example, H. A. Fertig, in *Perspectives in Quantum Hall Effects*, edited by S. Das Sarma and A. Pinczuk (Wiley, New York, 1997).

³ H. W. Jiang, R. L. Willett, H. Störmer, D. C. Tsui, L. N. Pfeiffer, and K. W. West, Phys. Rev. Lett. **65**, 633 (1990).

⁴ V. J. Goldman, M. Santos, M. Shayegan, and J. E. Cunningham, Phys. Rev. Lett. **65**, 2189 (1990).

⁵ H. W. Jiang, H. Störmer, D. C. Tsui, L. N. Pfeiffer, and K. W. West, Phys. Rev. B **44**, 8107 (1991).

⁶ M. B. Santos, Y. W. Suen, M. Shayegan, Y. P. Li, L. W. Engel, and D. C. Tsui, Phys. Rev. Lett. **68**, 1188 (1992).

⁷ C.-C. Li, L. W. Engel, D. Shahar, D. C. Tsui, and M. Shayegan, Phys. Rev. Lett. **79**, 1353 (1997).

- ⁸ C.-C. Li, J. Yoon, D. C. Tsui, M. Shayegan, and L. W. Engel, Proceedings of the 24th International Conference on the Physics of Semiconductors, 1998.
- ⁹ P. F. Hennigan, A. Beya, C. J. Mellor, R. Gaal, F. I. B. Williams, and M. Hnini, Proceedings of the 12th International Conference on the Electronic Properties of Two-Dimensional Systems, 1998.
- ¹⁰ H. Buhmann, W. Joss, K. von Klitzing, I. V. Kukushkin, A. S. Plaut, G. Martinez, K. Ploog, and V. B. Timofeev, Phys. Rev. Lett. **66**, 926 (1991).
- ¹¹ R. G. Clark, Physica Scripta **T39**, 45 (1991).
- ¹² I. V. Kukushkin, N. J. Pulsford, K. von Klitzing, K. Ploog, R. J. Haug, S. Kock, and V. B. Timofeev, Phys. Rev. B **45**, 4532 (1992).
- ¹³ I. V. Kukushkin, V. I. Fal'ko, R. J. Haug, K. von Klitzing, K. Eberl, and K. Totemayer, Phys. Rev. Lett. **72**, 3594 (1994).
- ¹⁴ E. M. Goldys, S. A. Brown, R. B. Dunford, A. G. Davies, R. Newbury, R. G. Clark, P. E. Simmonds, J. J. Harris, and C. T. Foxon, Phys. Rev. B **46**, 7957 (1992).
- ¹⁵ H. Fukuyama and P. A. Lee, Phys. Rev. B **18**, 6245 (1978).
- ¹⁶ B. G. A. Normand, P. B. Littlewood, and A. J. Millis, Phys. Rev. B **46**, 3920 (1992).
- ¹⁷ R. Chitra, T. Giamarchi, and P. Le Doussal, Phys. Rev. Lett. **80**, 3827 (1998).
- ¹⁸ H. A. Fertig, Phys. Rev. B **59**, 2120 (1999).
- ¹⁹ K. Maki and X. Zotos, Phys. Rev. B **28**, 4349 (1983).
- ²⁰ A related model was studied using the Hartree-Fock approach in R. Côté and A. H. MacDonald, Surf. Sci. **263**, 187 (1992).
- ²¹ L. Bonsall and A. A. Maradudin, Phys. Rev. B **15**, 1959 (1977).
- ²² R. Côté and A. H. MacDonald, Phys. Rev. Lett. **65**, 2662 (1990).
- ²³ R. Côté and A. H. MacDonald, Phys. Rev. B **44**, 8759 (1991).
- ²⁴ W. Kohn, Phys. Rev. **123**, 1242 (1961).
- ²⁵ J. Schwinger, *Quantum Theory of Angular Momentum* (Academic, New York, 1965).
- ²⁶ A. Auerbach, *Interacting Electrons and Quantum Magnetism* (Springer, New York, 1994).
- ²⁷ C. Timm, S. M. Girvin, and P. Henelius, Phys. Rev. B **58**, 1464 (1998).
- ²⁸ H. Fukuyama, Solid State Commun. **17**, 1323 (1975).
- ²⁹ S. Conti and G. Vignale, cond-mat/9801318 (unpublished).
- ³⁰ L. Brey, N. F. Johnson, and B. I. Halperin, Phys. Rev. B **40**, 10 647 (1989).
- ³¹ S. K. Yip, Phys. Rev. B **43**, 1707 (1991).
- ³² It should be noted that a static homogeneous MF solution is not always the right choice. For example, if there is nesting, including an oscillatory part may give us a mean-field state that is lower in energy. [See I. Affleck and J. B. Marston, Phys. Rev. B **37**, 3774 (1998).] However, there is no reason to believe such is the case in our problem.
- ³³ See, for example, G. D. Mahan, *Many-Particle Physics*, (Plenum Press, New York, 1981), Chap. 3, Sec. 5.
- ³⁴ Recently, the authors of Refs. 7 and 8 have found that $\Delta\omega$ is actually at least one order of magnitude smaller than previously reported, if a lower power external ac field is used as a probe. [C.-C. Li (private communication); J. Yoon (private communication); D. C. Tsui (private communication).] As of this writing, the line width has not saturated yet and the final result is most likely to be further reduced.
- ³⁵ H. A. Fertig and R. Côté, Phys. Rev. B **48**, 2391 (1993).
- ³⁶ M. M. Fogler and D. A. Huse, cond-mat/9904245 (unpublished).